

# Ultrasensitive detection of toxic cations through changes in the tunnelling current across films of striped nanoparticles

Eun Seon Cho<sup>1,2†</sup>, Jiwon Kim<sup>3†</sup>, Baudilio Tejerina<sup>3</sup>, Thomas M. Hermans<sup>3</sup>, Hao Jiang<sup>4</sup>, Hideyuki Nakanishi<sup>3</sup>, Miao Yu<sup>2</sup>, Alexander Z. Patashinski<sup>3</sup>, Sharon C. Glotzer<sup>4</sup>, Francesco Stellacci<sup>1,2★</sup> and Bartosz A. Grzybowski<sup>3★</sup>

**Although multiple methods have been developed to detect metal cations, only a few offer sensitivities below 1 pM, and many require complicated procedures and sophisticated equipment. Here, we describe a class of simple solid-state sensors for the ultrasensitive detection of heavy-metal cations (notably, an unprecedented attomolar limit for the detection of CH<sub>3</sub>Hg<sup>+</sup> in both standardized solutions and environmental samples) through changes in the tunnelling current across films of nanoparticles (NPs) protected with striped monolayers of organic ligands. The sensors are also highly selective because of the ligand-shell organization of the NPs. On binding of metal cations, the electronic structure of the molecular bridges between proximal NPs changes, the tunnelling current increases and highly conductive paths ultimately percolate the entire film. The nanoscale heterogeneity of the structure of the film broadens the range of the cation-binding constants, which leads to wide sensitivity ranges (remarkably, over 18 orders of magnitude in CH<sub>3</sub>Hg<sup>+</sup> concentration).**

Many cations are toxic, posing serious consequences for the environment and for human health. As an example, organomercury species (for instance, methylmercury (II); refs 1,2) are extremely dangerous and cause neurological disorders such as Minamata disease<sup>3,4</sup>, and cadmium poisoning results in kidney and/or liver failure, bone softening and other ill effects (for example, Itai-itai disease<sup>5,6</sup>). Therefore, sensitive and selective detection of toxic metal cations is of paramount importance in assessing water pollution and in the elimination of potentially serious health and environmental hazards<sup>7–9</sup>. There are multiple approaches to detect these ions, including atomic absorption spectroscopy<sup>10,11</sup> and inductively coupled plasma spectroscopy<sup>12,13</sup> (ICP), a host of optical methods (colorimetric<sup>14,15</sup> or fluorescence-based assays<sup>16,17</sup> and systems based on surface plasmon resonance<sup>18,19</sup> or surface-enhanced Raman scattering<sup>20,21</sup>), and electrochemical methods<sup>22,23</sup>. Frequently, however, these methods require a sophisticated chemistry to incorporate host materials, such as macrocyclic rings (crown ethers, calixarenes or porphyrins), metal-ion-recognizable proteins, nucleic acids and polymers. Moreover, the sensitivity of these methods is insufficient<sup>24–27</sup> in several situations of public health concern (for example, accumulation of low picomolar concentrations of CH<sub>3</sub>Hg<sup>+</sup> and Cd<sup>2+</sup> in fish<sup>28,29</sup>). Furthermore, host-guest chemistries are not available for all cations, with CH<sub>3</sub>Hg<sup>+</sup> being a prominent example<sup>2</sup>.

Here we show that gold nanoparticles (Au NPs) coated with binary mixtures of *n*-hexanethiol (HT) and alkanethiols terminated with *n* = 1, 2 or 3 ethylene glycol (EG) units have a striped ligand structure (Fig. 1a,b) that generates supramolecular

pockets able to selectively trap ions, and that on such trapping the electron-conduction mechanism through films of these NPs changes markedly<sup>30</sup>. We implement these findings in a solid-state sensor of unmatched sensitivity: HT/EG<sub>3</sub> NPs sense CH<sub>3</sub>Hg<sup>+</sup> selectively and with a detection limit of ~1 aM, HT/EG<sub>2</sub> NPs sense ~1 pM concentrations of Cd<sup>2+</sup>, and HT/EG<sub>1</sub> NPs are ~1 nM sensors for Zn<sup>2+</sup>.

Au NPs ( $d = 4.7 \pm 0.9$  nm) were synthesized as described previously<sup>31,32</sup> (see Methods) and were functionalized with alternating stripes (Fig. 1a) of HT and EG<sub>*n*</sub> thiols (HS-(CH<sub>2</sub>)<sub>6</sub>-(OCH<sub>2</sub>CH<sub>2</sub>)<sub>*n*</sub>-OH, ultrapure grade, ProChimia). These striped NPs were examined by scanning tunnelling microscopy (STM): the width of both HT and EG<sub>2</sub> stripes was  $\sim 1.3 \pm 0.1$  nm (Fig. 1b). For control experiments, we prepared NPs coated with disordered HT/EG<sub>*n*</sub> mixed self-assembled monolayers (SAMs; random NPs (ref. 33)), but with the same relative content of the two thiols as in the striped NPs (see Supplementary Section S1), and also NPs covered with one-component SAMs of EG<sub>*n*</sub> thiols. All types of NPs were dispersed in methanol with a concentration of 2 mM of Au atoms. To fabricate the sensors, Au electrodes (30 nm thick, 5 mm long) were sputter-coated onto a glass substrate using a shadow mask; the gap between the two electrodes was typically  $w = 50$  μm wide and  $l = 5$  mm long (Fig. 1c). Approximately 3 μl of the Au NP solution was drop-cast onto the patterned glass and dried for two days in vacuum conditions to give NP films about  $H \sim 150$  nm thick (determined by profilometry for each sample); in this way, the number of NPs between the electrodes was of the order of 10<sup>11</sup> (Fig. 1d). To prevent re-dissolution of the film on exposure

<sup>1</sup>Department of Materials Science and Engineering, Massachusetts Institute of Technology, Cambridge, Massachusetts 02139, USA, <sup>2</sup>Institute of Materials, Ecole Polytechnique Fédérale de Lausanne (EPFL), 1015, Switzerland, <sup>3</sup>Department of Chemical and Biological Engineering and Department of Chemistry, Northwestern University, 2145 Sheridan Road, Evanston, Illinois 60208, USA, <sup>4</sup>Department of Chemical Engineering and Department of Materials Science and Engineering, University of Michigan, Ann Arbor, Michigan 48109-2136, USA. <sup>†</sup>These authors contributed equally to this work.

\*e-mail: francesco.stellacci@epfl.ch; grzybor@northwestern.edu.

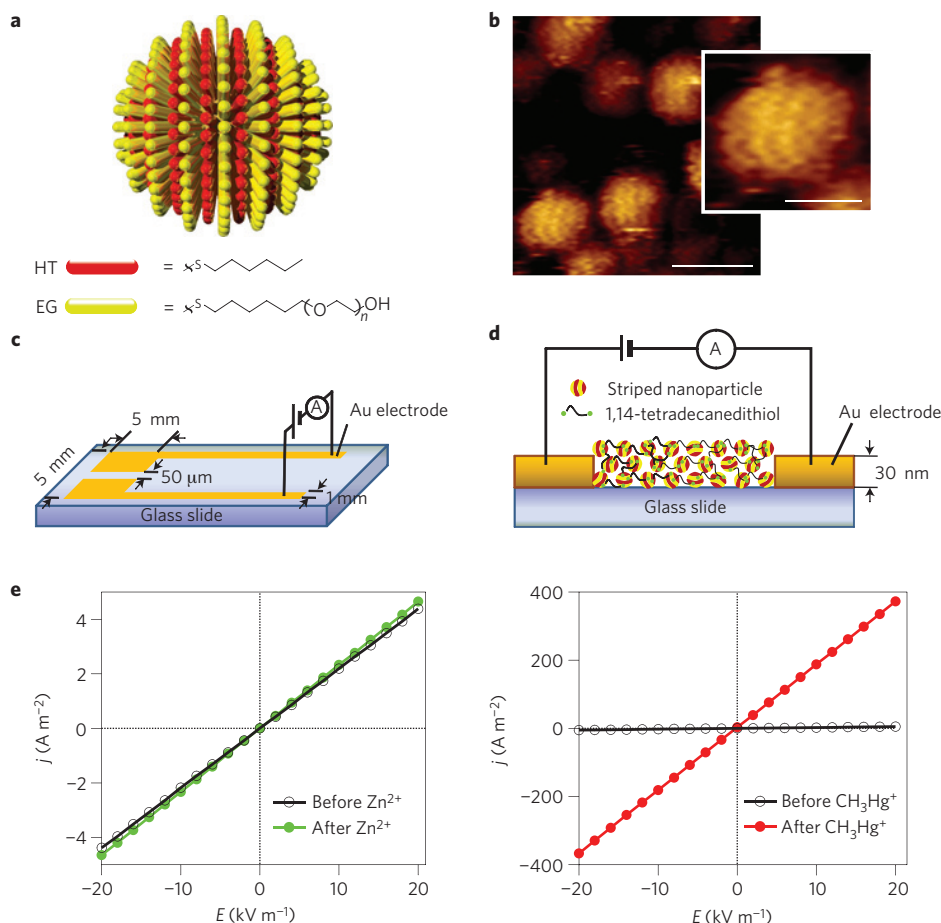


**Figure 1 | Experimental set-up and typical  $j$ - $E$  plots.** **a,b**, An idealized scheme of a striped nanoparticle (**a**) and the corresponding STM image (here, for HT/EG<sub>2</sub> NPs) obtained by a Veeco multimode scanning probe microscope on a vibration damping table (in an acoustic chamber, at room temperature, and in air; **b**). Scale bars, 10 nm (main image) and 5 nm (inset). **c,d**, The scheme and the dimensions of the device (**c**) and the side view of the NP film (**d**). **e**, Ohmic current density versus applied field,  $j$ - $E$ , and dependencies for a film of striped HT/EG<sub>3</sub> Au NPs before exposure to cations (black circles) and after exposure to cations (coloured circles). In the graph on the left, the conductance of the films is virtually unchanged after immersion in a 1 mM solution of Zn<sup>2+</sup> (green circles). In the graph on the right, immersion of the same film in a 1 mM solution of CH<sub>3</sub>Hg<sup>+</sup> (red circles) results in a marked change in the conductance (note the difference in the  $j$  ranges in the two plots).

to solvent, the film was reinforced by crosslinking the NPs with 1,14-tetradecanedithiol (dithiol concentration: 5 mM in toluene, crosslinking time: 40 min; for details see refs 34–36). Subsequently, the films were washed with an excess of toluene, dried under a stream of Ar, and then placed in vacuum conditions for two days. After drying the solvent, the Au electrodes were connected to a high-precision Keithley 6517 electrometer housed in a home-made Faraday cage (to minimize the effects of static electricity). The films were subsequently immersed in 2 ml of solutions of K<sup>+</sup>, Na<sup>+</sup>, Zn<sup>2+</sup>, Cd<sup>2+</sup>, Cs<sup>+</sup>, CH<sub>3</sub>Hg<sup>+</sup>, Co<sup>2+</sup>, Hg<sup>2+</sup>, Pb<sup>2+</sup>, Cu<sup>2+</sup>, Ni<sup>2+</sup>, Tl<sup>+</sup>, Ca<sup>2+</sup>, Ag<sup>+</sup> and CH<sub>3</sub>Zn<sup>+</sup> chloride salts in ultrapure water (resistivity: 18.2 MΩ cm) with concentrations ranging from 1 mM down to 1 zM (zeptomolar, 10<sup>-21</sup> M; note, the nature of the anions of the salts used, for example, chlorides versus bromides, had no effect on the results described below). The films were kept immersed in these solutions for  $t \sim 120$  s. This time was sufficient for the ions to penetrate the full depth of the film,  $H$ —using a conservative estimate of the diffusion coefficient of ions/small molecules in a nanoporous material,  $D \sim 10^{-14}$  m<sup>2</sup> s<sup>-1</sup> (ref. 37), the diffusion depth can be estimated as  $\sqrt{Dt} \sim 1 \mu\text{m}$ , which is greater than  $H$ . Consequently, the conductivities of the films discussed below did not change for longer immersion times. After immersion, the films were washed with copious amounts of water to remove excess salt and were then thoroughly dried under a stream of nitrogen. All

subsequent measurements were performed at room temperature ( $T \sim 300 \pm 2$  K), under dry air in a hermetic Faraday cage, and in the presence of desiccant (phosphorous pentoxide, P<sub>2</sub>O<sub>5</sub>; the presence of the desiccant, however, had no noticeable effect on the results).

The current density–applied field ( $j$ - $E$ ) dependencies for all types of films/cations were recorded for fields up to 20 kV m<sup>-1</sup> (higher fields cause irreversible changes in the NP films and coalescence of the neighbouring nanoparticles<sup>30</sup>). In this range, the  $j$ - $E$  dependencies were ohmic (Fig. 1e) and the conductivities of the films,  $\sigma = j/E$ , were constant for a given film type or condition (see Methods and Supplementary Section S2 for typical  $j$ - $V(t)$  curves at various concentrations of CH<sub>3</sub>Hg<sup>+</sup>). Before the immersion into the salt solutions, the conductivities of the striped EG<sub>*n*</sub> particle films were  $\sigma_{\text{before}} \sim 2 \times 10^{-4} \Omega^{-1} \text{m}^{-1}$ , which is close to the values previously recorded for films of Au NPs covered with thiolate SAMs of comparable thickness<sup>30</sup>. The conductivities increased (to  $\sigma_{\text{after}}$ ) when the films were exposed to the cations (Fig. 1e). The degree of this increase depended crucially on the nature of the SAM coating the NPs, and on the nature and the concentration of the cations (Fig. 2). In all cases, the sensitivity of the sensors was defined as the concentration of cations in solution at which the ratio of the conductivities of the NP film,  $\chi = \sigma_{\text{after}}/\sigma_{\text{before}}$ , was greater than unity at the 99% confidence level (for statistical analysis, see Supplementary Section S3).

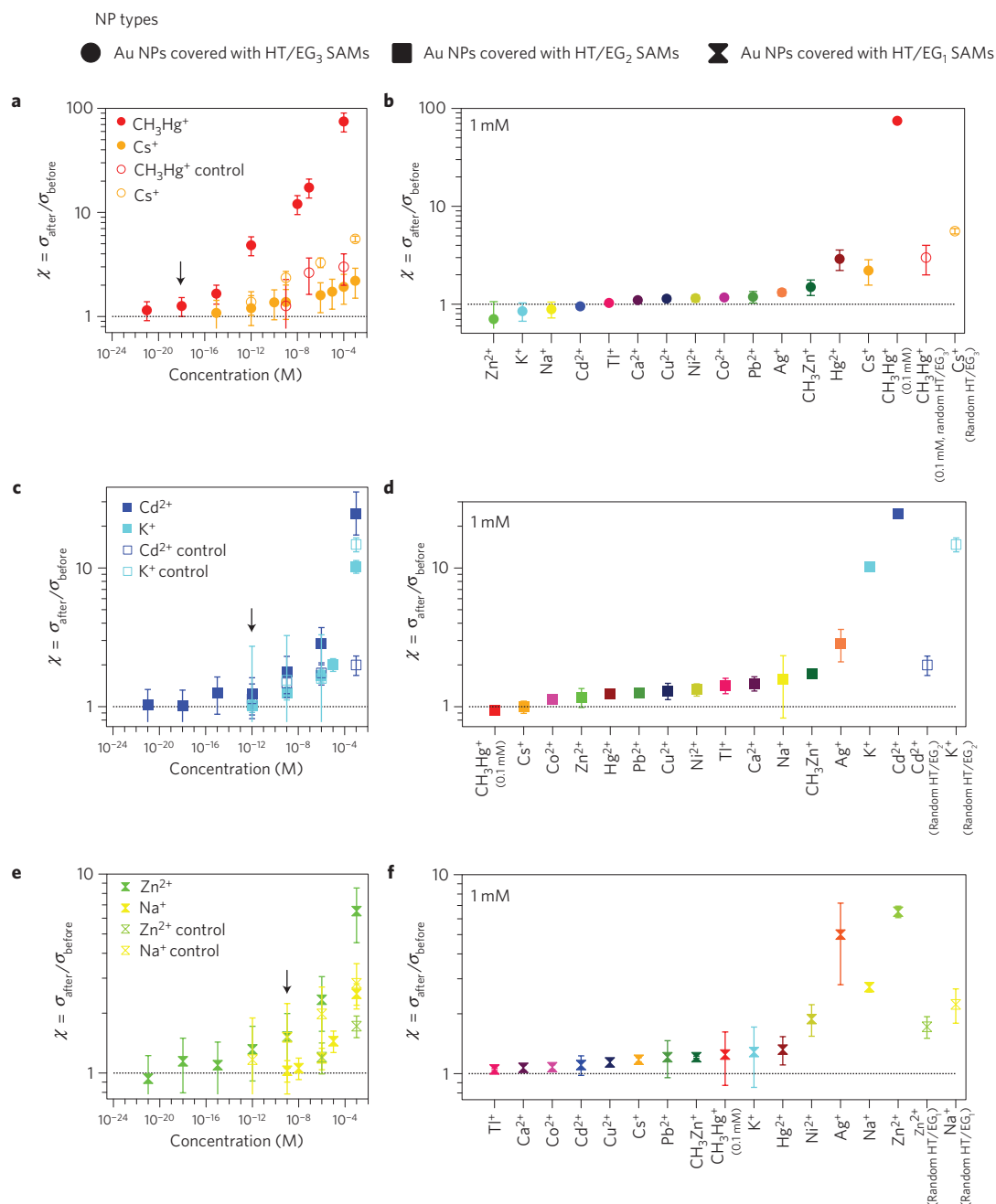


**Figure 2 | Sensitivity (left column) and selectivity (right column) of cation sensing by different types of Au NPs decorated by HT/EG<sub>n</sub> SAMs.**

These measures are quantified by the change in the conductivities of the films on cation exposure,  $\chi = \sigma_{\text{after}}/\sigma_{\text{before}}$ . Filled symbols correspond to nanoparticles covered with striped HT/EG<sub>n</sub> SAMs; open symbols correspond to control experiments in which the nanoparticles were covered with disordered/non-striped SAMs of the same composition. Standard deviations are for at least 12 independent experiments for each condition. The arrows in the left column point to the detection limit/sensitivity (defined in the main text; see also Supplementary Section S3). **a,b**, Au NPs covered with HT/EG<sub>3</sub> SAMs detect CH<sub>3</sub>Hg<sup>+</sup> selectively with a detection limit of ~1 aM. **c,d**, HT/EG<sub>2</sub> Au NPs detect Cd<sup>2+</sup> and K<sup>+</sup> with a detection limit of ~1 pM for both cations. **e,f**, HT/EG<sub>1</sub> Au NPs detect Zn<sup>2+</sup> and also Na<sup>+</sup> (detection limits: ~1 nM and ~1 μM, respectively). Note that the plots in **a, c** and **e** are double logarithmic and the conductivity increases nonlinearly with cation concentration.

Specifically, the HT/EG<sub>3</sub> striped Au NPs detected methyl mercury, CH<sub>3</sub>Hg<sup>+</sup>, with an approximately attomolar (10<sup>-18</sup> M) sensitivity limit (corresponding to only ~600 CH<sub>3</sub>Hg<sup>+</sup> cations in 1 ml of the surrounding solution; Fig. 2a). As the concentration of methyl mercury increased,  $\chi$  increased nonlinearly with [CH<sub>3</sub>Hg<sup>+</sup>] and reached a value of ~75 at [CH<sub>3</sub>Hg<sup>+</sup>] = 0.1 mM. Moreover, these sensing characteristics were selective for methyl mercury (Fig. 2b). For Co<sup>2+</sup>, Pb<sup>2+</sup>, Cu<sup>2+</sup>, Ni<sup>2+</sup>, Tl<sup>+</sup>, Ca<sup>2+</sup>, Ag<sup>+</sup>, CH<sub>3</sub>Zn<sup>+</sup>, Cd<sup>2+</sup>, K<sup>+</sup>, Na<sup>+</sup>, Cs<sup>+</sup> and Zn<sup>2+</sup>, the conductivity did not change

perceptibly ( $\chi \approx 1$ ) over the entire range of concentrations tested; for Hg<sup>2+</sup> and Cs<sup>+</sup> it changed only slightly ( $\chi < 2.9$  and  $\chi < 2.21$ , respectively). Furthermore, for Cs<sup>+</sup>, the detection limit was only ~1 μM—that is, 12 orders of magnitude above that of CH<sub>3</sub>Hg<sup>+</sup>.

Films of Au NPs coated with striped SAMs of HT/EG<sub>2</sub> detected Cd<sup>2+</sup> with  $\chi = 24.7$  at 1 mM and a detection limit ~1 pM (Fig. 2c,d). These NPs, however, also detected K<sup>+</sup> with  $\chi = 10.2$  at 1 mM and with ~1 pM detection limit and, to a lesser degree, Ag<sup>+</sup>

**Table 1 | Film sensitivity and energies in cation complexation.**

NP types	$\chi^{\text{binding}}$	$\chi^{\text{non-binding}}$	$\chi^{\text{mixture}}$
HT/EG <sub>3</sub>	$\chi^{\text{Cs}^+} = 1.600 \pm 0.512$	$\chi^{\text{Na}^+} = 0.888 \pm 0.165$	$\chi^{\text{Cs}^+/\text{Na}^+} = 1.671 \pm 0.389$
HT/EG <sub>2</sub>	$\chi^{\text{Cd}^{2+}} = 2.859 \pm 0.858$	$\chi^{\text{Zn}^{2+}} = 1.170 \pm 0.182$	$\chi^{\text{Cd}^{2+}/\text{Zn}^{2+}} = 2.373 \pm 1.238$
HT/EG <sub>1</sub>	$\chi^{\text{Zn}^{2+}} = 2.337 \pm 0.716$	$\chi^{\text{Cd}^{2+}} = 1.105 \pm 0.125$	$\chi^{\text{Zn}^{2+}/\text{Cd}^{2+}} = 2.406 \pm 0.383$

Sensitivity (that is,  $\chi = \sigma_{\text{after}}/\sigma_{\text{before}}$ ) in binary mixtures comprising cations that bind (denoted in bold) to the NPs and cations that do not bind (not bold). No significant differences between  $\chi^{\text{binding}}$  and  $\chi^{\text{mixture}}$  were observed. Standard deviations are for at least six independent experiments for each condition.

with  $\chi = 2.86$ . On the other hand, they did not bind  $\text{Co}^{2+}$ ,  $\text{Pb}^{2+}$ ,  $\text{Cu}^{2+}$ ,  $\text{Ni}^{2+}$ ,  $\text{Tl}^+$ ,  $\text{Ca}^{2+}$ ,  $\text{CH}_3\text{Zn}^+$ ,  $\text{Na}^+$ ,  $\text{Zn}^{2+}$ ,  $\text{Cs}^+$  and  $\text{CH}_3\text{Hg}^+$ . Finally, Au NPs coated with striped SAMs of HT/EG<sub>1</sub> were least selective and detected  $\text{Zn}^{2+}$ ,  $\text{Ag}^+$  and  $\text{Na}^+$  (Fig. 2e,f). In this case, the values of  $\chi$  were rather moderate (for example, at 1 mM, 6.51 for  $\text{Zn}^{2+}$ , 5.00 for  $\text{Ag}^+$  and 2.72 for  $\text{Na}^+$ ) although the sensitivity towards  $\text{Zn}^{2+}$  remained relatively high (for example, detection limit  $\sim 1$  nM versus  $\sim 1$   $\mu\text{M}$  for  $\text{Na}^+$ ). We note that Au NPs coated with random/non-striped HT/EG<sub>n</sub> SAMs were significantly less sensitive and in most cases less selective in detecting the highest- $\chi$  cations (but not some lower- $\chi$  cations, see open symbols in Fig. 2). Also, particles coated only with pure EG<sub>n</sub> SAMs exhibited even lower values of  $\chi$  (for details, see Supplementary Section S4).

We emphasize that all  $\chi$  values discussed above reflect the effects of cation binding and not any water and/or drying effects. This was verified in a series of experiments in which the films were washed in cation-free, deionized water and then dried—in this case, no statistically significant changes in the conductivities of the films were observed after either one or multiple wash/dry cycles (for example, for HT/EG<sub>2</sub> Au NP films,  $\chi = \sigma_{\text{after}}/\sigma_{\text{before}} = 1.011 \pm 0.029$  after one cycle and  $1.013 \pm 0.031$  after ten cycles). Also, when the cations were first captured into the films (such that conductivities increased) but were then washed off (by placing the films in 80 °C deionized water for 2–3 h), the conductivities returned to their native values before cation capture (see Supplementary Section S7). We observe that the films owe their robustness during all of these experiments (see Supplementary Section S6) to the crosslinking of the NPs by dithiols; films in which the NPs were not crosslinked simply dissolved when washed with or immersed in water.

The changes in the conductivity of the film result from the capture of the cations by the ligands on the NPs. This was directly verified by means of the ICP and X-ray photoelectron spectroscopy analyses of NPs before and after ion capture (see Supplementary Section S5 for these and other techniques used). In addition, Fourier transform infrared spectroscopy studies were performed that evidenced spectral changes on cation binding. Of particular importance here were the changes in the characteristic vibrational modes of the ethylene glycol units at 1001–1003  $\text{cm}^{-1}$  and at 827  $\text{cm}^{-1}$ . Remarkably, these changes were reversible in the sense that the original spectra were retrieved when the cations were washed off the NPs during immersion in 80 °C water (see above). These results also indicate that the capture of the cations is mediated by coordination-type interactions with the EG units, as should indeed be expected on the basis of common chemical knowledge. It is also worth noting that cations for which  $\chi = \sigma_{\text{after}}/\sigma_{\text{before}}$  is close to unity do not cause significant changes in the NP/NP-film spectra as discussed in the Supplementary Section S5. Interestingly, a qualitatively similar result is obtained from solution experiments where the conductivities of NP suspensions are monitored during titration with different salt solutions. For those salts that are characterized by low  $\chi$  in our solid-state (that is, NP-film) measurements, the conductance of NP solutions increases linearly

with the amount of salt added; for those, however, that exhibit higher  $\chi$  in NP films, the solution conductance initially remains constant, indicating that the added cations are trapped on the NPs (and thus do not contribute to the conductance of the solution; see Supplementary Section S5.5).

An essential feature of any chemical sensor is its selectivity, which in our case needs to be determined on exposure of NP films to cation mixtures. We first consider binary mixtures comprising cations that the NP films bind and sense with statistical significance (that is, giving conductance ratios  $\chi = \sigma_{\text{after}}/\sigma_{\text{before}} > 1$  at 99% confidence levels) and cations that do not bind strongly and do not change conductivities at such confidence levels. Such pairs correspond to most of the possible combinations among the cations we tested (see Fig. 2). The results for some representative pairs are summarized in Table 1. Specifically, for the HT/EG<sub>3</sub> Au NP films, the presence of weakly binding  $\text{Na}^+$  does not significantly change the signal coming from stronger binding  $\text{Cs}^+$ . Similarly, for HT/EG<sub>2</sub> Au NP films, the presence of  $\text{Zn}^{2+}$  does not strongly affect the signal due to  $\text{Cd}^{2+}$ , and for HT/EG<sub>1</sub> Au NP films the conductance on exposure to the mixture of  $\text{Zn}^{2+}$  and  $\text{Cd}^{2+}$  is close to the value characterizing the former cation. Such data confirm the selectivity of the films towards cations giving larger values of  $\chi$ . Moreover, the signals from the NP-film sensors are not affected by the changes in the ionic strength of the solution due to the non-binding, low- $\chi$  cations (see Supplementary Fig. S9a).

Of course, the selectivity decreases when the films are exposed to mixtures of cations characterized by similar  $\chi > 1$  values (Supplementary Section S12). This problem is the least pronounced for HT/EG<sub>3</sub> Au NP films (see Fig. 2 and Supplementary Section S8), which are therefore suitable for deployment as environmental  $\text{CH}_3\text{Hg}^+$  sensors. This is illustrated in Fig. 3, where we used our sensors to measure the  $\text{CH}_3\text{Hg}^+$  content in environmental samples directly relevant to the issues of public health—tap water, lake water and fish (see Methods for detailed preparation and analysis of environmental samples). Importantly, the results we obtained for the lake water could be directly compared to the values reported in the literature for the same lake (Lake Michigan) sample, and the  $\text{CH}_3\text{Hg}^+$  content in fish could be compared to the value determined by the United States Geological Survey (USGS). For the lake water, our measurements gave a 5.9 fM concentration of  $\text{CH}_3\text{Hg}^+$  (range within one s.d. 0.35–43.3 fM) versus 5–210 fM reported in ref. 38. For the fish, we measured a concentration of 3.81 pM (range within one s.d.: 1.62–8.19 pM), in excellent agreement with the 3.58 pM value provided to us by the USGS after our experiments were completed. A reassuring result—at least for the citizens of Evanston—is that the content of  $\text{CH}_3\text{Hg}^+$  in the tap water of this city is very low (27.7 aM, range within one s.d.: 4.5–138 aM). We make two further comments about all of these results. First, when the environmental samples were spiked with known concentrations of  $\text{CH}_3\text{Hg}^+$ , the readings of our films fell onto the calibration curve obtained using the concentration standards (that is, solutions of  $\text{CH}_3\text{Hg}^+$  in pure, deionized water)—this means that there is no background interference from components other than  $\text{CH}_3\text{Hg}^+$  in the environmental samples. Second, we emphasize that our







